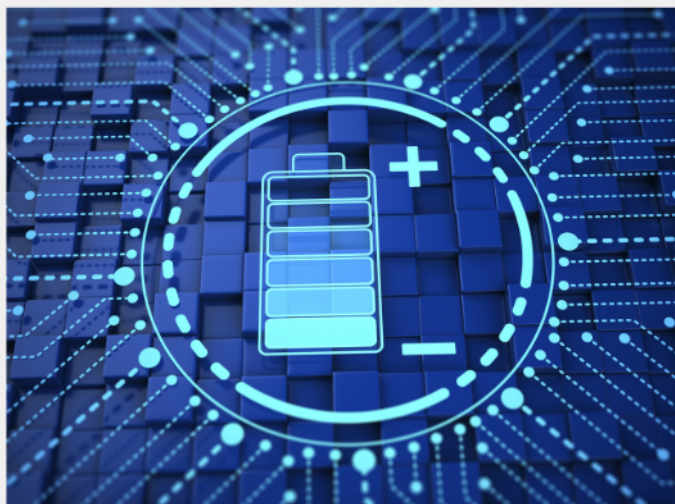# Exploring the possibilities of increasing energy density and efficiency in rechargeable batteries

Download this complimentary article collection

The exponential rise in the need for better, more efficient power sources has sparked an incredible amount of research into batteries. A primary focus of research has been increasing the energy density of batteries, as it allows for lighter, more portable storage of energy. Lithium-ion batteries, for example, have a much higher energy density than conventional lead-acid batteries and can be used for various purposes, such as in electric vehicles.

This article collection provides a comprehensive list of references for new methods and technologies for increasing the energy density of batteries.

Metrohm

WILEY

Stretchable Strain Sensors Based on Deterministic-Contact-Resistance Braided Structures with High Performance and Capability of Continuous Production

Juyao Li, Shuang Li, and Yewang Su*

Owing to their potential applicability in wearable devices and intelligent robots, stretchable strain sensors have been widely investigated. However, fabricating sensors with high sensitivity, wide sensing range, high repeatability, robustness, and capability for continuous production remains challenging. Herein, a deterministic-contact-resistance braided structure (DCRBS)-based stretchable strain sensor is proposed. The polyester yarns in the sensor tightly trap the silver fibers with the latex thread substrate to form a periodic "Y" structure to avoid slippage of the fibers, thereby facilitating deterministic contact and separation between the silver fibers during cyclic stretching. Owing to this braided structure, the strain sensor exhibits high repeatability (repeatability error = 3.74%), high sensitivity (gauge factor up to 140), wide sensing range (50%), and high robustness (washability, insensitivity to micro-defects). Additionally, the strain sensor can be continuously mass produced using mature raw materials and processing technology. Because of its demonstrated excellent performance, the strain sensor can find applications in human motion monitoring, rehabilitation medicine, and robotic control.

1. Introduction

Recently, smart wearable devices integrated with various sensors have attracted considerable attention owing to their wide applications in human-machine interaction,[1–3] sports performance monitoring,[4,5] medical treatment,[6] etcetera. Stretchable strain sensors are crucial in monitoring full-range human body motions[7,8] including small deformations, such as breathing, pulse, and muscle movement, and large deformations in joints, such as finger joints, elbows, and knees. The sensing range of traditional strain gauges is generally within

5%,[9,10] which is practically inapplicable. Stretchable strain sensors for smart wearable devices should possess the following fundamental characteristics:[11] 1) *Wide sensing range.* To measure large deformations of human joints, the sensing range of strain sensors must be greater than 50%. 2) *Appropriate high sensitivity (gauge factor).* This facilitates the measurement of weak deformation signals, such as pulses, and prevents large measuring errors. 3) *High repeatability.* This is essential for the accurate response of a strain sensor to a signal under cyclic stretching. 4) *Robustness.* Robustness, including washability, abrasion resistance, insensitivity to micro-defects, and the ability to withstand extreme loads, is crucial for applications in smart wearable devices. 5) *Capability for low-cost and continuous production.* This is crucial for widespread commercial application. 6) Other important optional performances depending on the specific application scenario, such as high linearity, fast response/recovery time, low drift and relaxation, temperature insensitivity, etc.

Stretchable strain sensors of the resistance type have the advantages of simple constitution, anti-environmental disturbance, etc. Most studies have focused on the following three strategies for the design and fabrication of stretchable strain sensors: a) *Microcrack-based stretchable strain sensors.*[12,13] This strategy involves the development of new conductive materials, such as graphene,[14–16] carbon nanotubes,[17] carbon black,[18] silver nanowires,[19] reduced graphene oxide[20] encapsulated by stretchable substrates, such as polydimethylsiloxane (PDMS),[21] Ecoflex,[22] thermoplastic polyurethane (TPU).[23] During stretching, variations in the relationship between microcrack surfaces in the conductive material cause a resistance change in the strain sensors that usually have a wide sensing range and high sensitivity (gauge factor). However, their repeatability is insufficient[24] because of the randomness of microcracks and unstable contact relationships involving continual microcrack propagation. b) *Textile-based stretchable strain sensors.*[25–27] These sensors are usually constructed using conductive fibers with a single knitted,[28–30] braided or woven structure[31–33] in which variations in the contact relationship yield resistance change. Because well-defined structures and contact relationships are adopted, the repeatability of

J. Li, S. Li, Y. Su
State Key Laboratory of Nonlinear Mechanics
Institute of Mechanics
Chinese Academy of Sciences
Beijing 100190, China
E-mail: yewangsu@imech.ac.cn
J. Li, S. Li, Y. Su
School of Engineering Science
University of Chinese Academy of Sciences
Beijing 100049, China

The ORCID identification number(s) for the author(s) of this article can be found under https://doi.org/10.1002/adfm.202208216.

**ADVANCED
SCIENCE NEWS**

www.advancedsciencenews.com

**ADVANCED
FUNCTIONAL
MATERIALS**

www.afm-journal.de

textile-based stretchable strain sensors is marginally better than that of microcrack-based strain sensors;[34,35] however, the fiber bundles of these structures are weakly constrained by each other and prone to slippage under the applied strain and yield drift of the electric response. Low cost and continuous production are significant advantages of textile-based stretchable strain sensors. c) *Contact resistance-free stretchable strain sensors*. To improve the repeatability of stretchable strain sensors, Li et al. proposed a novel design based on a contact-resistance-free structure, i.e., an off-axis serpentine sandwich structure with a stretch-bending-stretch transformation mechanism.[36] Excellent repeatability (repeatability error = 1.58%) is guaranteed because the microstructures are completely deterministic, and neither unstable contact resistance nor plastic behavior occur during the sensing process (applied strain up to 50%). However, according to a recent theoretical study, the gauge factor (≈0.005) of the sensor is not optimal,[37] and microfabrication processes such as lithography and etching are not conducive in realizing low-cost and continuous production. Therefore, it is significant but challenging to develop a stretchable strain sensor with a wide sensing range, appropriately high sensitivity, high repeatability, and capability for continuous production.

In this study, a stretchable strain sensor based on a deterministic contact resistance braided structure (DCRBS) has been proposed. In DCRBS, the polyester yarns tightly bind the silver fibers and latex threads to form a periodic "Y" structure, which prevents slippage between the fibers during stretching, thereby resulting in small relaxation and high repeatability of the strain signal. The contact area of silver fibers of the strain sensor varies significantly during the stretching process causing high sensitivity (gauge factor of up to 140). The strain sensor has a wide sensing range (50%) that can realize all-range measurement of human motion signals. Profiting from the DCRBS, the strain sensor has high robustness, including insensitivity to

micro-defects, excellent washability, and wear resistance. Additionally, the strain sensor uses mature raw materials and industrial processing technology, which guarantees continuous mass production. This paper discusses representative application scenarios of strain sensors, including human motion signal monitoring and risk warning, injury rehabilitation, and robotic control. All test results indicate that the proposed stretchable strain sensor exhibits excellent performance, a wide sensing range, high sensitivity, repeatability, robustness, low cost, and easy integration into clothing for its applicability in wearable electronic devices.

2. Results and Discussion

2.1. Design and Fabrication of the Stretchable Strain Sensors Based on the DCRBS

As shown in **Figure 1**a, the following three raw materials are required to fabricate the stretchable strain sensors: latex threads with a diameter of 150 μm, silver fibers, and polyester yarns with sizes of 210D/36F and 150D/48F (D denotes Denier, mass grams of 9000 m-long fibers at convention moisture regain; 36F represents 36 filaments in a bundle of fibers). These materials possess the advantages of water washability, abrasion resistance, biocompatibility, and well-established industrial fabrication processes. The fabrication process of stretchable strain sensors is illustrated in Figure 1a. The rubber latex threads are pre-stretched to the elastic limit by applying a strain of 150%; thereafter, the silver fibers are woven onto the rubber latex threads as weft yarns that are used as warp yarns to bind the silver fibers and latex threads using a knitting method. The release of the applied strain on the rubber latex threads yields contact between adjacent silver fibers. In the formed deterministic structures, the rubber latex
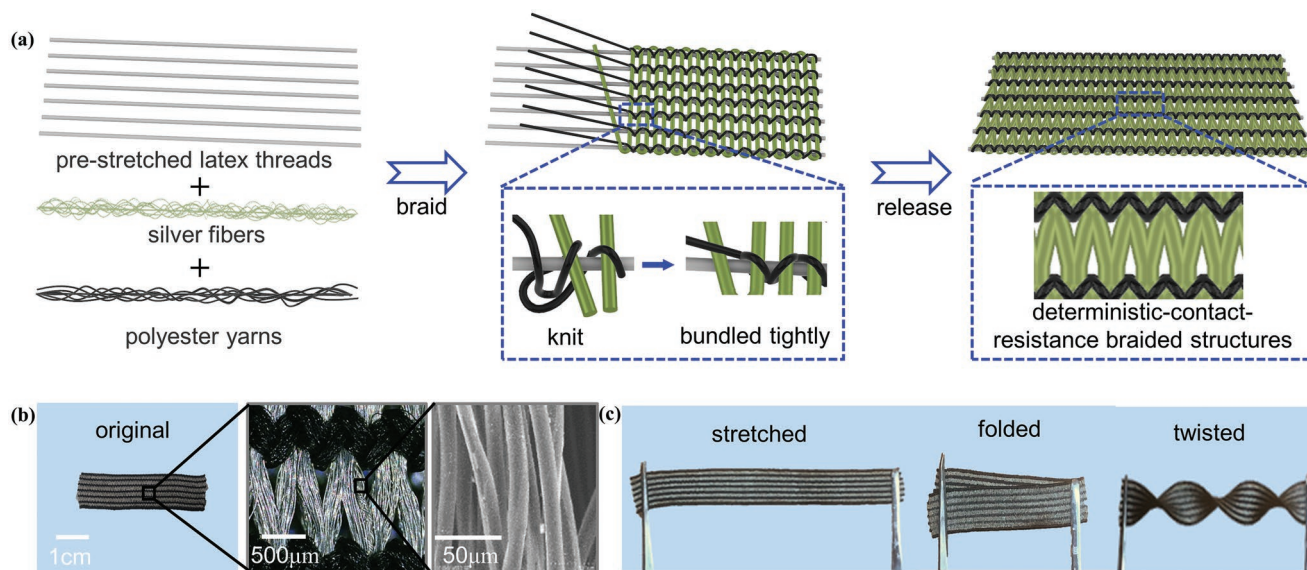

Figure 1. Fabrication process and images of the DCRBS-based strain sensor. a) Materials required to prepare the strain sensor: latex threads (grey), silver fibers (green), polyester yarns (black), and the schematics of fabricating the strain sensor. b) Photographs of strain sensors on various scales. c) Stretched, folded, and twisted strain sensors.

**ADVANCED
SCIENCE NEWS**

www.advancedsciencenews.com

**ADVANCED
FUNCTIONAL
MATERIALS**

www.afm-journal.de

threads, silver fibers, and polyester yarns produce the elastic force, sensing function, and binding function, respectively. The deterministic structures would not loosen on applying various deformations and yield deterministic contact between adjacent silver fibers. Figure 1b shows the macro- and microstructures of the stretchable strain sensors. It can be observed that the surfaces of silver fibers are uniform and smooth (the right subgraph), which is facilitates the repeatability of stretchable strain sensors. As shown in Figure 1c, DCRBS-based stretchable strain sensors are stretchable, foldable,

and twistable, indicating the feasibility of their application in wearable electronic devices.

2.2. Basic Sensing Performance and Mechanism of DCRBS-Based Stretchable Strain Sensors

Basic sensing performance tests were performed, and the corresponding theoretical model was established to further understand the sensor mechanism. **Figure 2**a shows the experimental
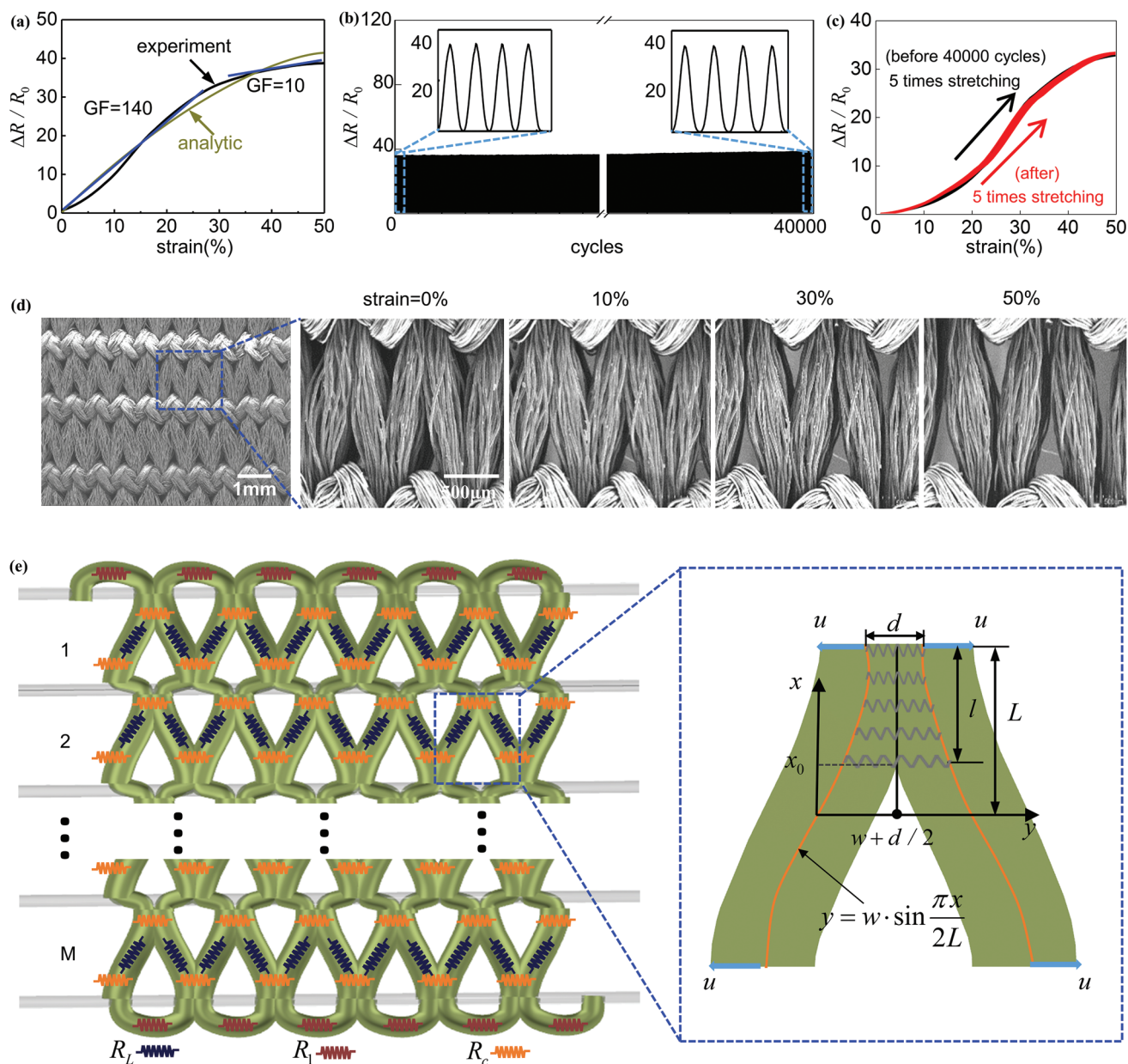

Figure 2. Basic sensing performance and mechanism of DCRBS-based strain sensors. a) Experimental and theoretical comparisons of the relationship between relative resistance and applied sensor strain. b) Durability and stability of the strain sensor under the cyclic strain of 50% for 40 000 cycles. c) The relationship between relative resistance changes and applied strain five times before (black lines) and after (red lines) 40000 cyclic loading, respectively. d) Microstructure and in situ tensile pictures of the sensor obtained using SEM. e) Schematics of the circuit and mechanical model of the strain sensor.

results of relative resistance of the stretchable strain sensor as a function of the applied strain (black line; the sensor width is 1 cm). The gauge factor (GF) of a strain sensor, defined as the slope of the curve of relative change in resistance versus applied strain, can be expressed using the following formula:

$$GF = \frac{d(\Delta R / R_0)}{d\varepsilon_{app}} \tag{1}$$

where ΔR is the change in resistance, R_0 is the initial resistance of strain sensor without strain, and ε_{app} is the applied strain. As shown in Figure 2a, DCRBS-based stretchable strain sensors have appropriately high GFs of 140 and 10 for strain in the ranges of 0–20% and 30%–50%, respectively. From the observations of Li et al.[37] on the influence of GF on measurement error, the ideal resolutions of a stretchable strain sensor are 2.4×10^{-6} and 1.0×10^{-6} for the applied strains of 20% and 40%, respectively (see Supporting Information for detail). This indicates that DCRBS-based stretchable strain sensors possess appropriately high sensitivities. Figure 2b shows the variation in relative resistance of the DCRBS-based stretchable strain sensor under 50% cycle-applied strain (loading frequency of 0.25 Hz). The insets in Figure 2b show the initial and final four cycles. After 40000 cycles, the signal of strain sensor did not change significantly, thereby demonstrating excellent repeatability and durability. To further verify the good repeatability of DCRBS-based stretchable strain sensors, Figure 2c shows the relationship between the relative resistance variation and applied strain five times before and after 40 000 cyclic loading. As shown in Figure 2d, the stretchable strain sensor exhibits high repeatability (repeatability error $\delta_R = 3.74\%$[38]) under 0–50% applied strain owing to its DCRBS. In addition, the strain sensor also exhibits excellent repeatability (repeatability error $\delta_R = 1.08\%$) under ultralow applied strain (1%), which is important for signal calibration and accurate measurement of small deformations (Figure S1, Supporting Information). The left subgraph of Figure 2d shows the overall microstructure of the stretchable strain sensor. The polyester yarns tightly bind the silver fibers on latex threads, and the two adjacent bundles of silver fibers are connected to form a periodic Y-shaped deterministic structure. Owing to the unique braided structure (as shown in the last three subgraphs of Figure 2d), greater applied strain causes stronger restraint between the silver fibers and latex threads by the polyester yarns. This significantly prevents slippage between silver fibers and ensures that the fibers deform uniformly with the stretching of latex thread substrate. This is the primary cause behind the high repeatability of DCRBS-based strain sensors.

As shown in the right sub-graph of Figure 2d and Figure S14 (Supporting Information), the contact range of two adjacent bundles of silver fibers gradually decreases with increase in the applied strain, causing an increase in the contact resistance and a further increase in the overall structure's resistance, thereby realizing the sensing of applied strain. To quantitatively study the sensing mechanism of stretchable strain sensors, a mechanical-electrical coupling model was established. Figure 2e shows the schematic structure and equivalent circuit diagram of the stretchable strain sensor, where R_1 represents the length-direction resistance of silver fibers in the periodic unit at the boundary of a strain sensor, R_L represents the length-direction resistance

of silver fibers in the periodic structure (part in the blue box), and R_c is the contact resistance between two adjacent bundles of silver fibers that varies with the applied strain. A schematic diagram of the theoretical model to quantitatively describe the relationship between them is presented in Figure 2e (right subgraph) and Figure S2 (Supporting Information). Owing to the confinement of polyester yarns, the silver fiber bundles exhibit a sinusoidal shape ($y = w \cdot \sin(\pi x / 2L), 0 \leq x \leq L$, where w is the magnitude of deflection of the silver fiber bundle axis, L is half the distance between two adjacent latex threads), and it is assumed that this configuration does not change during stretching. The tensile stiffness of the latex threads is much greater than that of the structure of silver fibers; thus, the tensile deformation of the latex threads is uniform under the applied strain. Both ends of the silver fiber bundles were loaded with displacement, and the interaction between silver fibers was assumed analogous to springs with the elastic coefficient k. Using the aforementioned conditions, the relationship between the contact length of adjacent fiber bundles and applied strain can be obtained as follows:

$$l = L - \frac{2L}{\pi}\arcsin\left(1 - \frac{d}{4w} + \frac{d}{2w} \cdot \varepsilon_{app}\right) \tag{2}$$

and the pressure between the fibers is,

$$p = k \cdot \left(w \cdot \sin\frac{\pi x}{2L} + \frac{d}{4} - \frac{1}{2}d \cdot \varepsilon_{app} - w\right) \tag{3}$$

where d is the distance between the center points of two adjacent silver-fiber bundles. According to the Holm contact law,[39] contact resistance is inversely proportional to the contact length and pressure. Thus, the contact resistance can be simplified as follows:

$$R_c = \frac{R_{c0}}{\overline{l} \cdot \overline{p}} + c \tag{4}$$

where R_{c0} and c are the fitting coefficients representing the initial contact resistance per unit length and effect of surface contact, respectively (in the actual situation, the two adjacent bundles of silver fibers are in surface contact, as shown in Figure 2d, and the model is simplified as line contact); $\overline{l} = l/L$ is the dimensionless contact length; $\overline{p} = \int_{x_0}^{L} p \cdot dx / (k \cdot w \cdot l)$ is the dimensionless average contact pressure; $x_0 = (2L/\pi)\arcsin\left[1 - d/(4w) + d/(2w) \cdot \varepsilon_{app}\right]$ is the abscissa of the critical point of contact between two adjacent bundles of silver fibers. By substituting these parameters into Equation (4), the contact resistance can be obtained as follows:

$$R_c = \frac{R_{c0}}{\cos\frac{\pi x_0}{2L} + \left(\frac{d}{4w} - \frac{d}{2w}\varepsilon_{app} - 1\right)\left(\frac{\pi}{2} - \frac{\pi x_0}{2L}\right)} + c \tag{5}$$

According to the circuit diagrams in Figure 2e and Figure S15 (Supporting Information), and Kirchhoff's voltage law,[40] the algebraic sum of the potential differences (voltages) across all elements along a closed loop is equal to zero. Thus, the fabric circuit network equations can be expressed as follows:

**ADVANCED
SCIENCE NEWS**

www.advancedsciencenews.com

**ADVANCED
FUNCTIONAL
MATERIALS**

www.afm-journal.de

$$
\begin{bmatrix}
2R_c + R_L & -R_c & 0 & \cdots & 0 & -R_L & 0 & \cdots & 0 & -R_c \\
-R_c & 2R_c + R_L & -R_c & & & & & & & 0 \\
0 & -R_c & \bullet & & & & -R_L & & & \bullet \\
\bullet & & & \bullet & & & & \bullet & & \bullet \\
\bullet & & & & \bullet & -R_c & & & \bullet & \\
0 & & -R_c & R_1 + R_c + R_L & 0 & & & -R_L & & 0 \\
-R_L & & & 0 & R_1 + R_c + R_L & -R_c & & & & -R_1 \\
0 & -R_L & & & -R_c & 2R_c + R_L & & & & 0 \\
\bullet & & \bullet & & & & \bullet & & \bullet & \\
\bullet & & & \bullet & & & & \bullet & & \\
0 & & -R_L & & & & & 2R_c + R_L & 0 & \\
-R_c & 0 & \bullet & \bullet & 0 & -R_1 & 0 & \cdots & 0 & R_1 + R_c
\end{bmatrix}
\begin{bmatrix}
i_1 \\ i_2 \\ i_3 \\ \bullet \\ \bullet \\ \bullet \\ \bullet \\ \bullet \\ \bullet \\ 0 \\ i_{2M+1}
\end{bmatrix}
=
\begin{bmatrix}
0 \\ 0 \\ 0 \\ \bullet \\ \bullet \\ \bullet \\ \bullet \\ \bullet \\ \bullet \\ 0 \\ U
\end{bmatrix}
\tag{6}
$$

where M is the number of intervals in the width direction of sensor, as shown in Figure 2e. Substituting the aforementioned contact resistance into the equivalent resistance to obtain the change in equivalent resistance with applied strain, as follows:

$$
\begin{aligned}
R_{\text{equ}} &= \frac{U}{i_{2M+1}} \\
&= \frac{2(4R_L^3 R_c^2 + 4R_1 R_L^3 R_c + 8R_L^2 R_c^3 + 12R_1 R_L^2 R_c^2 + 3R_1 R_c^4 + 9R_1 R_L R_c^3 + R_1 R_c^4)}{36R_L^3 R_c + 20R_1 R_L^3 + 76R_L^2 R_c^2 + 64R_1 R_L^2 R_c + 33R_1 R_c^3 + 51R_1 R_L R_c^2 + R_c^4 + 6R_1 R_c^3}
\end{aligned}
\tag{7}
$$

For the parameters, $R_1 = 0.1$ mΩ, $R_L = 0.3$ mΩ, $R_{c0} = 1$ mΩ, $c = -8.22$ mΩ, $d = w$ (according to the observation in Figure 2d), and $M = 6$, Figure 2a presents a comparison of the experimental and theoretical (green line) results of the relationship between the relative resistance and applied strain of the strain sensor (see Supporting Information for detail). The trends of the two results are consistent, validating the rationality of the theoretical model. The slight deviation between the two results can be attributed to neglecting the contact relationship between the fibers inside the model's silver fiber bundle. However, this does not affect the understanding of key sensing mechanism using the analytical model. Additionally, the sensor's sensing range and GF can be individually designed using the analytical model to satisfy the requirements of strain measurement in different scenarios.

2.3. Dynamic Performance and Robustness of the DCRBS-Based Stretchable Strain Sensors

To demonstrate the sensor's excellent performance and practical value, various properties of stretchable strain sensors were systematically tested and studied. **Figure 3**a shows the sensor's resistance change under an extremely small strain (<1%). The strain sensor was stretched to 0.1%, 0.2%, 0.3%, 0.5%, 0.7%, and 1% strain for 1 s. The relative change in the strain sensor's resistance exhibited a distinct step-like signal indicating its high resolution, which is crucial for accurate detection of tiny deformations. The tests were also performed for larger strains (5%, 10%, 20%, 30%, and 50%) held for 5 s each. As shown in Figure S3 (Supporting Information), the stretchable strain sensor can effectively monitor strains up to 50%, and the resistance signal remains stable under the corresponding strain without significant drift and relaxation. The most pronounced

drift was negligible (≈3.4% at 20% strain). The limitations of textile-based strain sensors are signal drift and relaxation owing to the fiber slippage and viscoelasticity of fabric materials.[41–43] The proposed strain sensors possess a small drift that mainly benefits from the DCRBS in which the polyester yarns tightly bind the silver fibers and latex threads at the intersection, thereby preventing slippage between the fibers. Furthermore, when the ultralow strain (1%) is applied on the strain sensor, the relative change in resistance ascends within a fast response time about 56 ms (Figure 3b). The 1% strain maintains for 10 s and is removed afterwards; the response of the sensor promptly recovered with a short duration of ≈96 ms (the actual response/recovery time is the measured response/recovery time subtracted by the time of the increased or decreased strain, and the time of the increased or decreased strain is ≈72 ms). In addition, some literatures define the recovery time as the time required for the sensor signal to stabilize.[17] The recovery time of the sensor calculated in this way is also given as ≈5.88 s. Figure 3c shows the variation in relative resistance of stretchable strain sensors with the applied strain at three different speeds (100, 300, and 500 mm s⁻¹). It can be observed that at different applied speeds, the relative change in resistance with applied strain is almost without a visible difference. Therefore, the strain sensor signal does not depend on the applied speed.

The tendency of a highly practical stretchable strain sensor to resist the influence of external factors cannot be ignored. Strain sensors are mainly used in smart clothing and subjected to different temperature effects in different environments. To investigate the effect of ambient temperature on a stretchable strain sensor, the variation in sensor's resistance was measured at intervals of 10 °C in the range of 10–50 °C, as shown in Figure 3d. Compared with the results in Figure 3b, the effect of a 40 °C temperature change on the sensor's resistance is less than that of the 0.1% strain. Therefore, the effect of temperature on the sensor was negligible. For special cases, it can be observed from Figure 3d that the effect of temperature on the sensor's resistance is approximately linear, and the temperature influence coefficient of the resistance is ≈0.0015 °C⁻¹. Practically, strain sensors undergo combined torsional and tensile deformation with clothing. To investigate the effect of complex deformation on stretchable strain sensors, torsion-tensile experiments were performed. Stretching tests were performed after twisting the sensor by certain angles (0°, 20°, 45°, 90°,
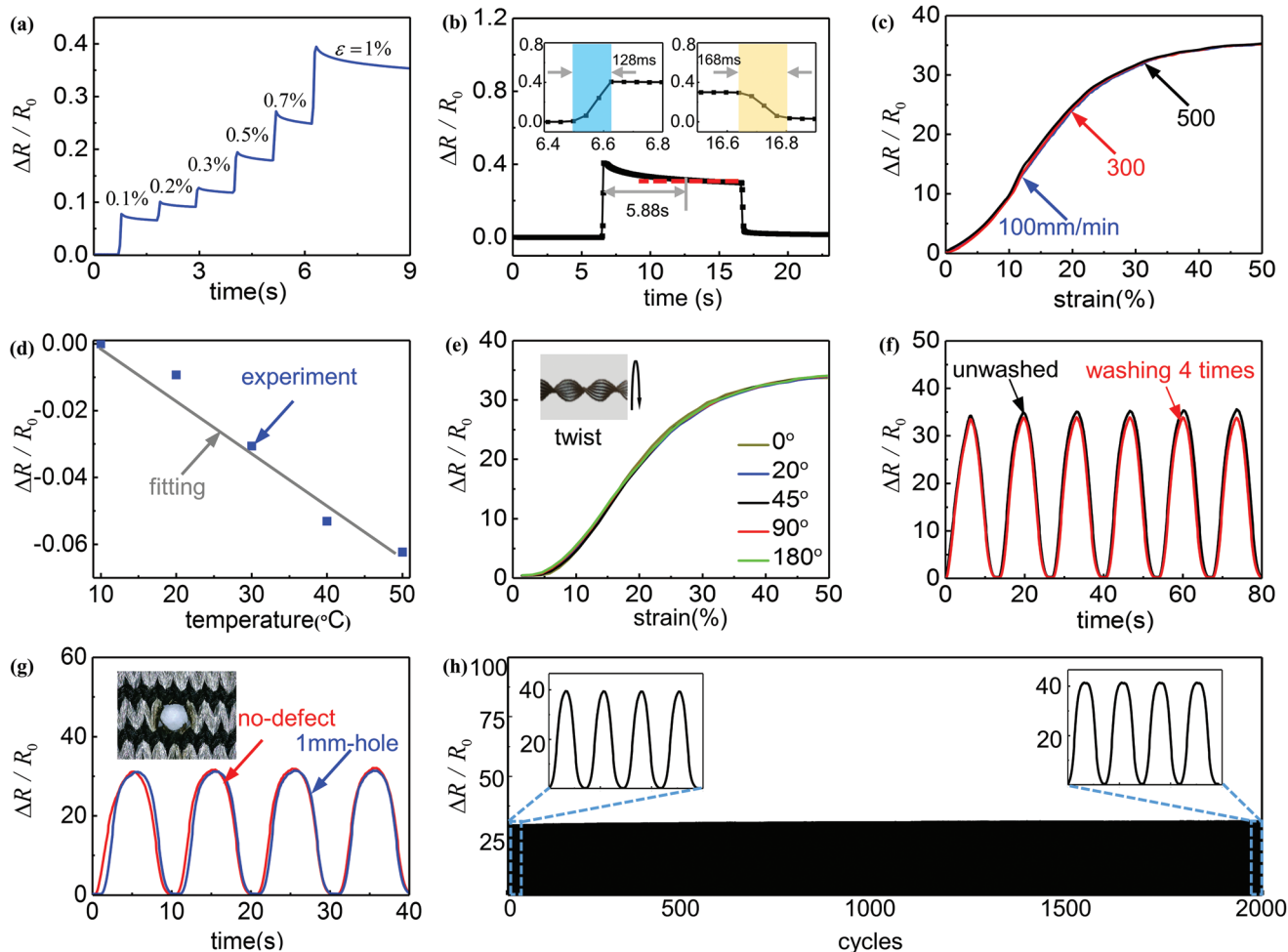
Figure 3. Dynamic performance and robustness of DCRBS-based strain sensors. a) Variation in the strain sensor's relative resistance versus time at various strains (0.1%, 0.2%, 0.3%, 0.5%, 0.7%, 1%). b) Response of the strain sensor to ultralow applied strain (1%). Insets: close-up of the response/recovery region. c) Variation in the strain sensor's relative resistance versus the applied strain at different stretching speeds (100, 300, 500 mm min⁻¹). d) Variation in the strain sensor's relative resistance versus the temperature. e) Effect of different twist angles (0°, 20°, 45°, 90°, 180°) on the strain sensor signal. f) Output signals of the strain sensor after washing 0 and 4 times. g) Relative resistance change responses of no-defect and defective strain sensors to 50% cyclic strain (the inset shows a strain sensor with a 1mm-hole). h) Durability and stability of the strain sensor with a 1mm-hole under the cyclic strain of 50% for 2000 cycles (insets show the variation in the strain sensor's relative resistance for the first and last four cycles).

180°), and the applied strain was 50%. Figure 3e shows the variation in sensor's relative resistance with respect to tensile strain at different twist angles. The response of the sensors to tensile strain is consistent under different twist angles, indicating that stretchable strain sensors can withstand combined deformation and be insensitive to twisting deformation but exhibit sensitivity to tensile deformation. The reason for insensitivity of the strain sensor to twisting is shown in Figure S4 (Supporting Information). The strain sensor with a length of 100 mm is twisted by 360°, and its microstructure and contact relationship is basically unchanged compared with that before twisting. Moreover, the strain sensors do not undergo extreme twisting under normal use, so the effect of twisting on the strain sensor can be ignored. Considering different directions of the applied forces on the wearable device, related experiments were performed to study the response of the strain sensor to normal and shear forces. As shown in Figure S5 (Supporting Information), the change of electrical signals generated by the weights of dif-

ferent masses pressing on the strain sensor is almost zero. To explore the effect of shear force on the strain sensor signal, the weights on the pre-stretched strain sensor (10%) were pushed from one end to another (A polyimide film was attached to the bottom of the weight to electrically insulate between the weight and the sensor). Figure S6 (Supporting Information) shows that the effect of shear force on the signal output of the strain sensor can be ignored, that is, the strain sensor is insensitive to shear force. Additionally, the washing durability of sensors is an important indicator that needs investigation. The sensors were placed in a washing machine for four wash cycles; Figure 3f shows the stretchable strain sensor's relative resistance under 50% strain cycling before and after the sensor was washed. Because the silver fibers have good washing resistance and periodic DCRBS can withstand extreme loads in a washing machine, no significant difference was observed between the two signal curves, thereby indicating that the sensor is washable. Abrasion and damage of textile-based strain sensors

during long-term service are inevitable. To study the effect of defects on stretchable strain sensors, a 1 mm hole was carved in the sensor using laser cutting, as shown in the insets of Figure 3g. On comparing the resistance signals of sensors with and without defects (Figure 3g), no obvious difference is observed. The effect of different damage locations on the sensor output signal is also considered. As shown in Figure S7 (Supporting Information), even if the polyester yarns are damaged, the effect on the performance of the strain sensor can be ignored. This is mainly due to the fact that the circuit of the strain sensor is multi-channel, and the size of the defect is much smaller than that of the sensor. Figure 3h shows the variation in resistance of a stretchable strain sensor with a 1 mm defect under 50% cycle strain at 500 mm s^{-1}. The insets of Figure 3h show the initial and final four cycles. After 2000 cycles, the sensor's signal did not vary significantly, indicating the remarkable repeatability and durability of stretchable strain sensors with defects. Because DCRBS polyester yarns restrict the movement of silver fibers, the defects are not easily expandable. Additionally, the strain sensor can withstand extreme loads, such as punctures from scissors and strikes from wrenches (Figure S8, Supporting Information). These experimental results verify that DCRBS-based strain sensors are highly robust, which is crucial in their practical applications. In addition, by comparison with recently reported textile-based strain sensors, the DCRBS-based strain sensor exhibits excellent overall performance (the detailed comparison with previous studies are presented in Table S1, Supporting Information).[31,32,44–47]

2.4. Representative Applications for Monitoring Human Activities, Medical Rehabilitation, and Robotic control

To demonstrate the applicability of stretchable strain sensors in wearable devices, a smart fitness suit was prepared by integrating sensors in the shoulders, elbows, and backs of sports tights (as shown in **Figure 4**a). The strain sensor is integrated into the clothing by sewing (The middle position of the sensor adopts a Z-shaped sewing structure for stretchability, and the two ends adopt a linear sewing structure), which not only ensures high repeatability and accuracy when the strain sensors are used to monitor human motion, but also does not cause damage to the garment and DCRBS. The strain sensor sewn to the clothing is cyclically stretched (30% applied strain), and its signal exhibits a high repeatability as shown in Figure S9 (Supporting Information). The suit can be used for real-time monitoring of the movements of various parts of the human body during the fitness process. The wrong exercise posture fails to achieve the expected effect and is prone to injury. Detecting whether a movement is standardized is often difficult; therefore, intelligent auxiliary exercise equipment is required. Figure 4b shows a comparison of three typical correct and incorrect motion poses. The squat, which is one of the most common fitness exercises, is an indispensable movement for practicing the human body's core strength. The correct squat posture should keep the back straight throughout the process; however, habitually bending over while squatting can cause injury. Dumbbell curls and lifts exercise the biceps and shoulders, respectively. If the movements do not attain the peak

value, effective stimulation of the muscles and muscle growth is difficult to achieve. Sweating is inevitable when exercising for a long time. To explore the effect of sweat on the strain sensors, the experimenter wore tights with strain sensors for 30 min of outdoor running. After exercise, the experimenter sweated to the point that the strain sensor was soaked. Figure S10 (Supporting Information) shows the response of the strain sensor to 30% cycling applied strain before and after exercise. Although sweat reduces the sensitivity of the sensor, the strain sensor can still respond to stretching deformation. For special needs, the strain sensor can be encapsulated with a polymer material (PDMS, Ecoflex, etc.) to avoid the influence of sweat or other body fluids on its signal response.

Stretchable strain sensors have potential applications in medical rehabilitation. Pulse is an important physiological signal that indicates the health of a human body. In traditional Chinese medicine,[48] pulse is used to determine the cause of a disease. Figure 4c indicates that the DCRBS-based strain sensor has a sufficiently high resolution to monitor the human pulse signal. As shown in the insets of Figure 4c, the stretchable strain sensor could accurately monitor the three important peaks in pulse signal: the peak of advancing wave T_1, the peak of reflected wave T_2, and the peak of dicrotic wave T_3. These three characteristic peaks indicate the cardiovascular system's health status. Three months after cervical spine surgery, rehabilitation exercises can be performed using cervical flexion and extension. While standing or sitting, the neck is tilted back to the maximum for 3–5 s, and then the head is lowered to the maximum for 3–5 s. As shown in Figure 4d, the strain sensor was used to monitor neck movements to avoid secondary injury. Early postoperative rehabilitation of the knee joint is crucial; if there is no reasonable rehabilitation treatment, the knee joint will be stiff, thereby limiting the patient's lifestyle and kinesthesis. Based on the patient's condition, the doctor will recommend them to flex and extend their knee from 90 ° to 120 °. To quantitatively obtain the bending degree of knee joint, a DCRBS-based stretchable strain sensor was attached to the knee to monitor the knee joint's movement (Figure 4e).

Stretchable strain sensors have applications in the field of robotic control. Figure 4f and Movie S1 (Supporting Information) show a set of gesture-controlled gloves based on stretchable strain sensors. The strain sensors were sewn to an ordinary fabric glove and connected to the chip to convert the electrical signal into digital and control the manipulator using Bluetooth. The smart glove can realize gesture recognition and control the manipulator to grab high-risk items, such as nuclear radiation items, to improve the safety of personnel (limited by the function of the manipulator, only the grabbing action is shown here).

3. Conclusions

In summary, a DCRBS-based stretchable strain sensor with high sensitivity, wide sensing range, high repeatability, and capability for continuous production was designed. The sensor's GF can attain a value of 140, which is favorable for weak signal monitoring of the human epidermis, such as pulse. The effective sensing range is greater than or equal to 50%,
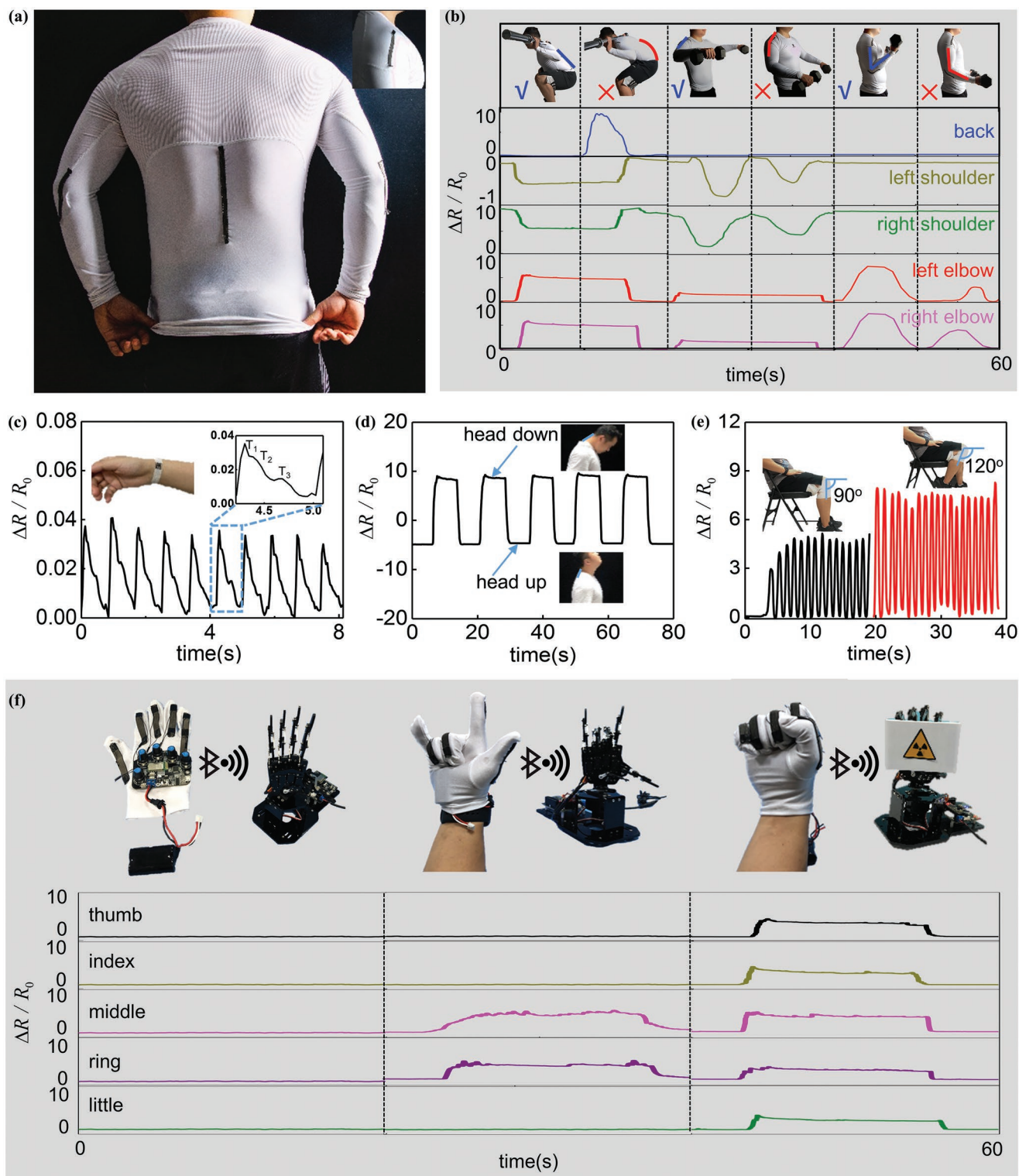
**ADVANCED
SCIENCE NEWS**

www.advancedsciencenews.com

**ADVANCED
FUNCTIONAL
MATERIALS**

www.afm-journal.de

Figure 4. Representative applications of the DCRBS-based strain sensor in smart wearable devices. a) Integration of the strain sensors with fitness suit (on shoulders, elbows and back). b) Correct and incorrect demonstrations of squats, dumbbell curls, dumbbell lateral raises and corresponding signals of sensors during fitness movements. c) Measurement of pulse signals by the strain sensor. d) Monitoring neck flexion and extension movements using the strain sensor. e) Monitoring knee joint rehabilitation exercise posture using the strain sensor. g) Wirelessly controlling the robotic palm and the corresponding electrical signals of smart glove sensors using strain sensors.

which is sufficient to monitor the movement of various joints in the human body. After undergoing a series of experimental tests, the sensor exhibited high repeatability and robustness, including washability, wear resistance, and insensitivity to defects. Additionally, the strain sensor has good compatibility with clothes and is easy to integrate. Owing to this, the prepared smart fitness clothing can accurately monitor the body's motion posture, which can be used to monitor the correctness of posture during fitness exercises, improve the exercise efficiency, and avoid injury. Notably, the raw materials of the stretchable strain sensor are commercially accessible and exhibit a stable performance. Furthermore, the processing technology of strain sensors is industrially well-established; therefore, continuous and scalable manufacturing can be realized. Hence, high-performance and continuously mass-produced DCRBS-based strain sensors are integral in the development of wearable smart products.

4. Experimental Section

Preparation of the Strain Sensor: A DCRBS-based stretchable strain sensor was fabricated using an MHW high-speed webbing machine (Minghai, China), as shown in Figure S11 (Supporting Information). Pre-stretched rubber latex threads (applied strain of ≈150%) were used as elastic basements, polyester fibers as warps, and silver fibers as wefts that are woven onto the latex threads of diameters 150 µm. The thickness of the polyester yarn was 150D, and the size of the silver fiber was 210D. Silver fibers were purchased from KAZHTEX Co., LTD (China).

Characterization of the Strain Sensors: Stretching tests of the stretchable strain sensors were conducted using programmable tensile testing machines (ZQ-990A, ZHIQU, China), as shown in Figure S12 (Supporting Information). The resistance signals of the sensors were measured using a digital multimeter (34972A; Keysight, USA).

Washing Test: The stretchable strain sensors were placed in a commercial washing machine (Midea, MB55-V3006G, China) with clothes. Each laundering cycle of ≈40 min duration consisted of the following four stages: washing, dehydration, rinsing, and dehydration. After several washes and natural drying, the electrical signals of sensors were measured.

Prefabricated Defects: A 1 mm micro-defect in the stretchable sensor was fabricated using a *P*-second laser precision machining system (DCT-DL566PU, China), as shown in Figure S13 (Supporting Information). The laser power was adjusted to 75% of the maximum and laser cutting was performed for 100 cycles.

Additional Experimental Details: The experiments involving human volunteers were approved by the Institutional Review Board at the Institute of Mechanics, Chinese Academy of Sciences (Approval No. 2022005), wherein the volunteers provided informed consent.

Supporting Information

Supporting Information is available from the Wiley Online Library or from the author.

Acknowledgements

Conflict of Interest

The authors declare no conflict of interest.

Authors Contribution

J.L. and Y.S. conceived the concept. J.L. conducted the experimental fabrication, theoretical derivation, and performance tests. J.L., S.L., and Y.S. discussed all the data. J.L., S.L. and Y.S. prepared the manuscript. Y.S. supervised the project.

Data Availability Statement

The data that support the findings of this study are available in the supplementary material of this article.

Keywords

[1] H. Bai, S. Li, J. Barreiros, Y. Tu, C. R. Pollock, R. F. Shepherd, *Science* **2020**, *370*, 848.

[2] H. Zhang, W. Han, K. Xu, Y. Zhang, Y. Lu, Z. Nie, Y. Du, J. Zhu, W. Huang, *Nano Lett.* **2020**, *20*, 3449.

[3] H. Zhang, W. Han, K. Xu, H. Lin, Y. Lu, H. Liu, R. Li, Y. Du, Z. Nie, F. Xu, L. Miao, J. Zhu, W. Huang, *Adv. Funct. Mater.* **2021**, *31*, 2009466.

[4] Q. Liu, M. Zhang, L. Huang, Y. Li, J. Chen, C. Li, G. Shi, *ACS Nano* **2015**, *9*, 12320.

[5] C. Tan, Z. Dong, Y. Li, H. Zhao, X. Huang, Z. Zhou, J. W. Jiang, Y. Z. Long, P. Jiang, T. Y. Zhang, B. Sun, *Nat. Commun.* **2020**, *11*, 3530.

[6] N. Luo, J. Zhang, X. Ding, Z. Zhou, Q. Zhang, Y. T. Zhang, S. C. Chen, J. L. Hu, N. Zhao, *Adv. Mater. Technol.* **2018**, *3*, 1700222.

[7] Q. Liu, J. Chen, Y. Li, G. Shi, *ACS Nano* **2016**, *10*, 7901.

[8] Y. Li, T. He, L. Shi, R. Wang, J. Sun, *ACS Appl. Mater. Interfaces* **2020**, *12*, 17691.

[9] D. J. Cohen, D. Mitra, K. Peterson, M. M. Maharbiz, *Nano Lett.* **2012**, *12*, 1821.

[10] M. Hempel, D. Nezich, J. Kong, M. Hofmann, *Nano Lett.* **2012**, *12*, 5714.

[11] J. Chen, J. Zhang, Z. Luo, J. Zhang, L. Li, Y. Su, *ACS Appl. Mater. Interfaces* **2020**, *12*, 22200.

[12] D. Kang, P. V. Pikhitsa, Y. W. Choi, C. Lee, S. S. Shin, L. Piao, B. Park, K. Y. Suh, T. Il Kim, M. Choi, *Nature* **2014**, *516*, 222.

[13] M. Amjadi, M. Turan, C. P. Clementson, M. Sitti, *ACS Appl. Mater. Interfaces* **2016**, *8*, 5618.

[14] Y. Wang, R. Yang, Z. Shi, L. Zhang, D. Shi, E. Wang, G. Zhang, *ACS Nano* **2011**, *5*, 3645.

[15] S. Bae, Y. Lee, B. K. Sharma, H. Lee, J. Kim, J. Ahn, *Carbon N. Y.* **2012**, *51*, 236.

[16] F. Han, J. Li, S. Zhao, Y. Zhang, W. Huang, G. Zhang, R. Sun, C. P. Wong, *J. Mater. Chem. C* **2017**, *5*, 10167.

[17] T. Yamada, Y. Hayamizu, Y. Yamamoto, Y. Yomogida, A. Izadi-Najafabadi, D. N. Futaba, K. Hata, *Nat. Nanotechnol.* **2011**, *6*, 296.

[18] X. Guo, Y. Huang, Y. Zhao, L. Mao, L. Gao, W. Pan, Y. Zhang, P. Liu, *Smart Mater. Struct.* **2017**, *26*, 095017.

[19] M. Amjadi, A. Pichitpajongkit, S. Lee, S. Ryu, I. Park, *ACS Nano* **2014**, *8*, 5154.

[20] Y. Liu, D. Zhang, *Compos. Sci. Technol.* **2016**, *137*, 102.

[21] T. Yang, X. Li, X. Jiang, S. Lin, J. Lao, J. Shi, Z. Zhen, Z. Li, H. Zhu, *Mater. Horiz.* **2016**, *3*, 248.

[22] Y. Zhang, X. Guo, W. Wang, L. Chen, L. Liu, H. Liu, Y. He, *IEEE Sens. J.* **2020**, *20*, 14118.

[23] R. Zhang, H. Deng, R. Valenca, J. Jin, Q. Fu, E. Bilotti, T. Peijs, *Compos. Sci. Technol.* **2013**, *74*, 1.

[24] Y. Y. Bai, B. Zhang, Z. X. Wang, Y. J. Yang, X. P. Wu, G. P. Zhang, *J. Mater. Chem. C* **2020**, *8*, 5202.

[25] S. Seyedin, P. Zhang, M. Naebe, S. Qin, J. Chen, X. Wang, J. M. Razal, *Mater. Horizons* **2019**, *6*, 219.

[26] G. M. N. Islam, A. Ali, S. Collie, *Cellulose* **2020**, *27*, 6103.

[27] J. Wang, C. Lu, K. Zhang, *Energy Environ. Mater.* **2020**, *3*, 80.

[28] W. Fan, Q. He, K. Meng, X. Tan, Z. Zhou, G. Zhang, J. Yang, Z. L. Wang, *Sci. Adv.* **2020**, *6*, eaay3111.

[29] H. Zhang, X. Tao, S. Wang, T. yu, *Text. Res. J.* **2005**, *75*, 598.

[30] R. Reddy K, S. Gandla, D. Gupta, *Adv. Mater. Interfaces* **2019**, *6*, 1900409.

[31] C. Luo, B. Tian, Q. Liu, Y. Feng, W. Wu, *Adv. Mater. Technol.* **2020**, *5*, 1900925.

[32] C. Wang, X. Li, E. L. Gao, M. Q. Jian, K. L. Xia, Q. Wang, Z. P. Xu, T. L. Ren, Y. Y. Zhang, *Adv. Mater.* **2016**, *28*, 6640.

[33] M. Zhang, C. Wang, H. Wang, M. Jian, X. Hao, Y. Zhang, *Adv. Funct. Mater.* **2017**, *27*.

[34] J. Lee, S. Shin, S. Lee, J. Song, S. Kang, H. Han, S. Kim, S. Kim, J. Seo, D. Kim, T. Lee, *ACS Nano* **2018**, *12*, 4259.

[35] Z. Yang, Y. Pang, X. L. Han, Y. Yang, Y. Yang, J. Ling, M. Jian, Y. Zhang, T. L. Ren, *ACS Nano* **2018**, *12*, 9134.

[36] S. Li, G. Liu, R. Li, Q. Li, Y. Zhao, M. Huang, M. Zhang, S. Yin, Y. Zhou, H. Tang, L. Wang, G. Fang, Y. Su, *ACS Nano* **2022**, *16*, 541.

[37] S. Li, G. Liu, L. Wang, G. Fang, Y. Su, *Adv. Electron. Mater.* **2020**, *6*, 2000618.

[38] O. A. M. A. H. Kara, *Pap. Knowl. Towar. a Media Hist. Doc.* **2014**, *7*, 107.

[39] R. Holm, *Electric Contacts*, Springer Berlin, Heidelberg **1974**.

[40] G. Zeng, M. Zeng, *Electric Circuits*, Springer Nature, Switzerland AG **2021**.

[41] O. Atalay, W. Richard Kennon, M. Dawood Husain, *Sensors* **2013**, *13*, 11114.

[42] A. Tewari, S. Gandla, S. Bohm, C. R. McNeill, D. Gupta, *Appl. Phys. Lett.* **2018**, *113*, 084101.

[43] G. Cai, M. Yang, Z. Xu, J. Liu, B. Tang, X. Wang, *Chem. Eng. J.* **2017**, *325*, 396.

[44] L. Wang, M. Tian, X. Qi, X. Sun, T. Xu, X. Liu, S. Zhu, X. Zhang, L. Qu, *Langmuir* **2021**, *37*, 3122.

[45] Z. Liu, Y. Zheng, L. Jin, K. Chen, H. Zhai, Q. Huang, Z. Chen, Y. Yi, M. Umar, L. Xu, G. Li, Q. Song, P. Yue, Y. Li, Z. Zheng, *Adv. Funct. Mater.* **2021**, *31*, 2007622.

[46] O. Atalay, *Materials* **2018**, *11*, 768.

[47] S. Yang, C. Li, X. Chen, Y. Zhao, H. Zhang, N. Wen, Z. Fan, L. Pan, *ACS Appl. Mater. Interfaces* **2020**, *12*, 19874.

[48] A. De Sá Ferreira, A. J. Lopes, *Chin. J. Integr. Med.* **2013**, *19*, 307.